Effects of Surface Pretreatment of Titanium Substrates on Properties of Electrophoretically Deposited Biopolymer Chitosan/Eudragit E 100 Coatings

Łukasz Pawłowski [1,*], Michał Bartmański [1], Aleksandra Mielewczyk-Gryń [2,3] and Andrzej Zieliński [1]

[1] Faculty of Mechanical Engineering and Ship Technology, Gdańsk University of Technology, 80-233 Gdańsk, Poland; michal.bartmanski@pg.edu.pl (M.B.); andrzej.zielinski@pg.edu.pl (A.Z.)

[2] Faculty of Applied Physics and Mathematics, Gdańsk University of Technology, 80-233 Gdańsk, Poland; alegryn@pg.edu.pl

[3] Advanced Materials Centre, Gdańsk University of Technology, 80-233 Gdańsk, Poland

* Correspondence: lukasz.pawlowski@pg.edu.pl; Tel.: +48-883-797-081

Abstract: The preparation of the metal surface before coating application is fundamental in determining the properties of the coatings, particularly the roughness, adhesion, and corrosion resistance. In this work, chitosan/Eudragit E 100 (chit/EE100) were fabricated by electrophoretic deposition (EPD) and both their microstructure and properties were investigated. The present research is aimed at characterizing the effects of the surface pretreatment of titanium substrate, applied deposition voltage, and time on physical, mechanical, and electrochemical properties of coatings. The coating's microstructure, topography, thickness, wettability, adhesion, and corrosion behavior were examined. The applied process parameters influenced the morphology of the coatings, which affected their properties. Coatings with the best properties, i.e., uniformity, proper thickness and roughness, hydrophilicity, highest adhesion to the substrate, and corrosion resistance, were obtained after deposition of chit/EE100 coating on nanotubular oxide layers produced by previous electrochemical oxidation.

Keywords: coatings; titanium; chitosan; eudragit; nanotubular titanium oxide; adhesion; thickness; topography; wettability; corrosion resistance

1. Introduction

The surface of titanium biomaterials for bone implants is usually subjected to modifications aimed at improving osteointegration properties, providing resistance to corrosion, or delivering a therapeutic substance to the perivascular tissues. For this purpose, the surface layer of the implant is modified or a specific coating is deposited [1–4]. The coatings for implants should be characterized by high adhesion to metallic substrates under shear stresses, suitable roughness, and high resistance to corrosion phenomena [5]. Nevertheless, such structures often exhibit a weak adhesion to the metallic substrate, which is exposed to heavy loads during the implantation procedure [6]. Coating delamination is one of the leading causes of the failure of biomedical implants with surface coatings [7]. The surface roughness of such systems is unfavorable for bonding the implant to the tissue or they degrade when exposed to the aggressive environments of the human body [8]. One of the key factors and which is rarely studied concerns the influencing of the properties of the produced layers and coatings as the method of pretreatment of the biomaterial surface before deposition [9,10].

There is a wide range of methods for implant surface preparation that affect its properties including, among others, surface roughness, surface charge, surface energy, and chemical composition. Such factors determine the performance of the deposited coatings

[11]. Among the methods of surface preparation, mechanical grinding [12,13], electrochemical polishing [14], etching [15,16], sandblasting [17,18], and chemical passivation [5,19] can be distinguished.

Dry or wet grinding are the most common and conventional mechanical methods of preparing implants before the coating deposition [20,21]. In using abrasive papers of a specific gradation, the desired surface roughness can be achieved [22]. Etching of the titanium surface provides a rougher surface and this method is frequently used for dental implants [23]. Acid etching is a subtraction method and the surface topography arises from a strong corrosion process, causing pits of different dimensions. During etching, the protective titanium oxide layer is dissolved, significantly altering the surface properties of the processed material [24]. There are reports regarding improved cell proliferation and bone formation after the etching of titanium samples [25,26]. Electrochemical anodizing is a technique that allows for obtaining self-organized, vertically oriented, and even nanotube structures on different metallic surfaces (e.g., zirconium, titanium, and titanium alloys). The growth of the nanotubes takes place through electrochemical processes and permits high control over the geometry of the structures' forms [27]. The resulted nanotubes of nanometric sizes are characterized by higher wettability and the ability to adsorb proteins from surrounding body fluids [28]. Moreover, these structures can reduce the adhesion of bacteria to the implant surface. The layer produced adheres strongly to the substrate, is difficult to scratch, and is not damaged when bending the substrate [29]. To further improve the osteointegration properties, the nanotubes may be modified by attaching various biomolecules to their surface. It is also possible to introduce a therapeutic substance into their interior, thus providing an effective drug delivery system [30]. The development of a surface treatment based on the removal of material by physical, chemical, and electrochemical methods is still under investigation. There are a variety of more advanced methods of pre-treatment for implant surfaces for coating deposition, such as micro-arc oxidation (MAO) [31], ion implantation [32], laser modification [33], and friction stir processing [34]; however, these methods are expensive and require more complex equipment [35].

The effect of substrate morphology on the final properties of the resulting coatings is seldom studied. Despite that, the beneficial effect of a neutral argon beam etching of 316L stainless steel, CoCr alloy, and Ti6Al4V on the adhesion of DLC (diamond-like carbon) coatings were confirmed [36]. The significant increase in adhesion of pure carbon coating to the Ti6Al4V substrate by carbon ion implantation was also investigated [37]. Subsequent treatments on the titanium surface, including grinding, etching in HNO_3/HF solution, sandblasting, soaking in NaOH, and subsequent heat treatment, provided an increasing adhesion trend of the deposited hydroxyapatite (HAp) coatings [38,39]. The increased bonding strength of the HAp coating to the titanium substrate was also observed after electrochemical oxidation of the metallic substrate and alkaline treatment of the nanotubular titania surface [40]. In addition, air abrasion coupled with chemical etching works synergistically to create strong bonds between PEEK-based (polyetheretherketone) polymers and dental adhesives [41].

Recently, smart coatings sensitive to external environmental conditions have attracted great interest [42–44]. Structures of this type are susceptible to changes in temperature, pH value, electric and magnetic field, or UV-VIS radiation [45]. Representatives of this group of materials are chitosan (chit) and Eudragit E 100 (EE100), which tend to be sensitive to pH drops. These biopolymers can form a system of controlled release of a therapeutic substance [46]. Previous studies on novel biopolymer coatings [47] have confirmed that the addition of Eudragit E 100 to chitosan coatings improves their stability in neutral pH, while maintaining high sensitivity to pH decline and improving the mechanical properties of these coatings. However, the adhesion of these coatings to the titanium substrate was still insufficient.

This study aims to determine the effect of the applied method of substrate surface preparation on the properties, especially roughness, adhesion, and corrosion resistance of

the electrophoretically deposited chit/EE100 coatings. The titanium grade 2 surface was subjected to grinding, etching, and electrochemical oxidation, and subsequently the chit/EE100 coatings' electrophoretic depositions using different process parameters were performed.

2. Materials and Methods

2.1. Substrate Pretreatment

The substrate used was Ti grade 2 (EkspresStal, Luboń, Poland). Its chemical composition given by the manufacturer is presented in Table 1. Round Ti grade 2 samples of a 12-mm diameter and 4-mm height (cut from the bar) were subjected to surface modification.

Table 1. The chemical composition of the Ti grade 2 substrate, wt.%.

Element	N	C	H	Fe	O	Ti
wt.%	0.009	0.013	0.001	0.168–0.179	0.170–0.190	rest

Samples for coating deposition were prepared in three different manners. The first pretreatment consisted of grinding the surface of the samples with SiC abrasive paper to the final gradation #800. Ground samples were degreased in isopropanol (99.7%, POCH, Gliwice, Poland) and washed with distilled water. The second modification involved etching samples of Ti grade 2 in hydrofluoric acid (10% HF, POCH, Gliwice, Poland) for 1 min and washing with isopropanol and distilled water. Finally, electrochemical anodization was performed according to the method described in previous studies [5]. The fabrication of the oxide nanotube layer was carried out in a solution containing 10 mL of 85% ortho-phosphoric acid (1 M H_3PO_4) (Sigma Aldrich, St. Louis, MO, USA), 1.2 mL of 40% hydrofluoric acid (POCH, Gliwice, Poland), and 150 mL of demineralized water. The tests were conducted using an electrical system consisting of a DC power source (MCP Corp., Shanghai, China), a platinum polarization electrode as a cathode, and a Ti grade 2 sample as an anode placed at a distance of 10 mm. The process was carried out at room temperature at a constant voltage of 20 V for 20 min. After oxidation, the samples were rinsed in distilled water and dried in the air at an ambient temperature for 24 h. Following the method of surface preparation, the samples were marked as G (ground), E (etched), or A (anodized), respectively.

2.2. Deposition of Chitosan/Eudragit E 100 Coatings

The electrophoretic deposition of chit/EE100 coatings was carried out according to the protocol described previously [47]. In short, an EPD suspension was prepared by dissolving 0.1 g of chitosan (coarse ground flakes and powder, purity > 99%, MW 310–375 kDa, degree of deacetylation > 75%; Sigma-Aldrich, St. Louis, MO, USA) and 0.25 g of Eudragit E 100 (purity 99.9%, MW 47 kDa, Evonik Industries, Darmstadt, Germany) in 100 mL of 1% acetic acid (99.9%, Stanlab, Gliwice, Poland) using a magnetic stirrer (Dragon Lab MS-H-Pro+, Schiltigheim, France) for 24 h. Using a setup similar to that for the electrochemical oxidation, the Ti substrate was employed as the cathode and the platinum mesh electrode as the anode. The distance between the electrodes was about 10 mm. The deposition was performed at an ambient temperature at 10 or 20 V, for 1 or 2 min. The characterization of each sample by the applied process parameters is shown in Table 2. After deposition, the samples were rinsed with distilled water and dried at an ambient temperature.

Table 2. Designations of experiment samples with the applied process parameters.

Sample	Substrate Pretreatment	Suspension	Voltage (V)	Time (min)
G1			10	1
G2				2
G1′	Grinding		20	1
G2′		100 mL of 1% *(v/v)* acetic acid with 0.1 g of chitosan and 0.25 g of Eudragit E 100		2
E1			10	1
E2				2
E1′	Etching		20	1
E2′				2
A1			10	1
A2				2
A1′	Anodization		20	1
A2′				2

2.3. Structure and Morphology Studies

The surfaces of the samples after the substrate pretreatment and further deposition of the coatings were examined by a scanning electron microscopy (SEM, JEOL JSM-7800F, JEOL Ltd., Tokyo, Japan). Before testing, the samples were sputtered with a 10-nm chromium layer using a DC magnetron sputtering system (Q150T ES, Quorum Technologies Ltd., Laughton, UK). The surface topography was examined with an atomic force microscope (NaniteAFM, Nanosurf AG, Liestal, Switzerland). A non-contact mode of examination was applied at a force set at 55 mN. The three tests carried out on an area of 50 × 50 µm were conducted. The surface topography parameters, i.e., arithmetic mean deviation (Sa), maximum peak height (Sp), and maximum valley depth (Sv), were determined. The thickness of the coatings was measured by a dual scope FMP100 coating thickness gauge (SN150001281, Helmut Fischer GmbH, Sindelfingen, Germany). Fifteen measurements were taken for each coated sample. The coatings were evaluated using an X-ray energy dispersion spectrometer (EDS, Edax Inc, Mahwah, NJ, USA) to detect the crystalline phases. Fourier-transform infrared spectroscopy (FTIR) using the Perkin Elmer spectroscope (Perkin Elmer Frontier, Waltham, MA, USA) in ATR mode with a resolution of 2 cm^{-1} in the range of 400–4000 cm^{-1} was employed to analyze the chemical bonds in the investigated materials.

2.4. Wettability Study

The falling drop method was performed to measure the water contact angle (Attention Theta Life, Biolin Scientific, Espoo, Finland) at room temperature. Five measurements were made for each sample. The volume of distilled water droplets was about 2 µL and the angle was measured 10 s after the droplet.

2.5. Adhesion Study

Adhesion of the chit/EE100 coatings to a metallic substrate was determined by a scratch test using the NanoTest™Vantage device (Micro Materials, Wrexham, UK). Scratches were made over a distance of 500 µm with increasing the load from 0 to 120 mN at a load speed of 1.3 mN/s. For each measurement, the force causing the complete delamination of the coating from the substrate was determined based on the sudden change in friction force as observed in the normal force vs. friction graph. In addition, all scratches were examined using an optical microscope (BX51, OLYMPUS, Tokyo, Japan).

2.6. Corrosion Study

Electrochemical measurements included the determination of the open circuit potential (OCP) of a system consisting of a platinum counter electrode, a calomel reference electrode, and a coated sample, placed in a simulated body fluid (SBF, prepared according to [48]) at 37 °C for 1 h. Subsequently, electrochemical impedance spectroscopy (EIS) was performed in the frequency range of 0.1 Hz–100 kHz with RMS = 10 mV. Corrosion curves in the −1.0–1.0 V range at a potential change rate of 1 mV/s were determined using the potentio-dynamic method. Based on the Tafel extrapolation, the values of the corrosion potential (E_{corr}) and the corrosion current density (i_{corr}) were found. All tests were conducted using a potentiostat/galvanostat (Atlas 0531, Atlas Sollich, Gdańsk, Poland).

3. Results and Discussion

3.1. Structure and Morphology Studies

Figure 1 depicts the morphology of Ti grade 2 substrates prepared for coating deposition with various surface pretreatment approaches such as grinding, etching, and electrochemical oxidation. In Figure 1a, typical structures resulting from the grinding process were visible [49]. Using acid etching, the oxide layer was removed and produced a more irregularly textured surface of the titanium substrate (Figure 1b) [24]. After etching, a surface with fairly sharp micro edges was acquired. Similar morphology was reported in a previous study [7]. During etching, hydrogen fluoride readily reacted with Ti and both titanium fluoride and hydrogen gas were formed [50]. SEM images showed residues from the etched surface layer that were not removed by washing the samples with isopropanol and distilled water. Images (Figure 1c) at higher magnifications revealed a nanotube oxide layer produced by electrochemical oxidation that covered the surface of the titanium sample [51].
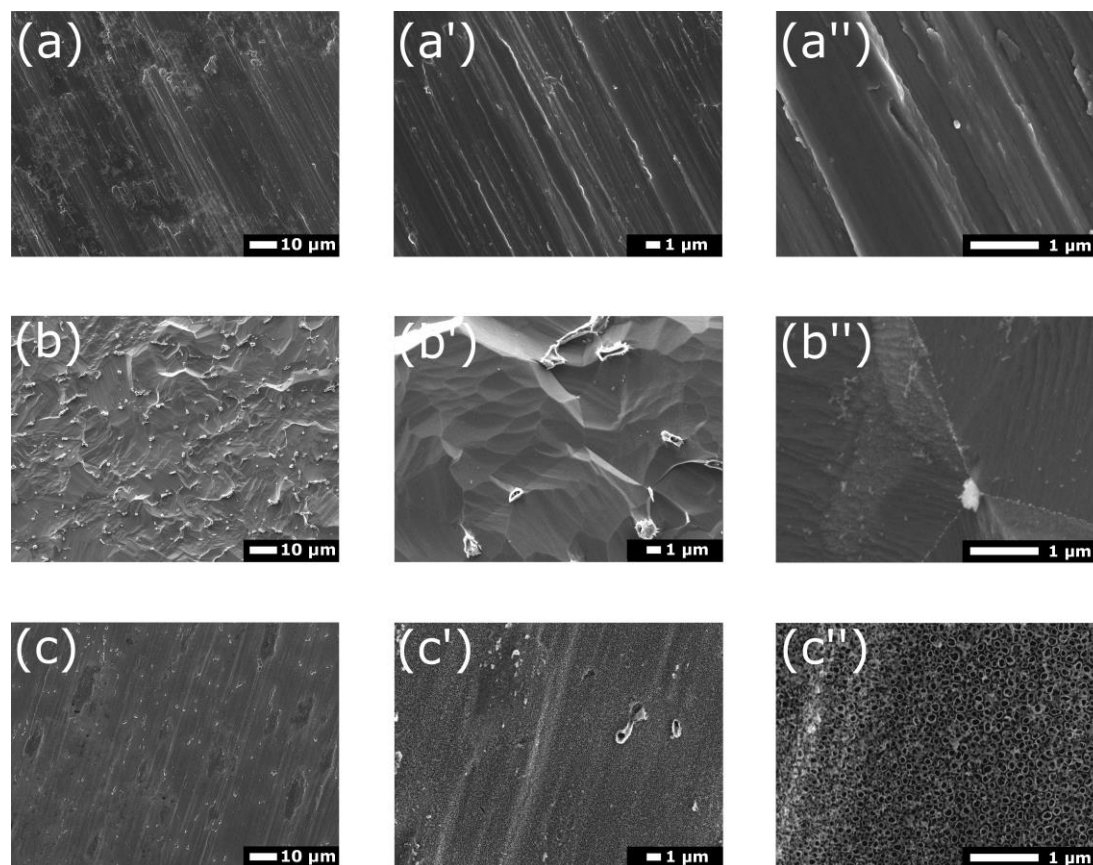

Figure 1. SEM images of surface pretreated Ti grade 2 substrates after (**a**) wet grinding, (**b**) acid etching, and (**c**) electrochemical anodization in different magnifications: ×1000 (a–c), ×5000 (a'–c'), and ×25000 (a''–c'').

The morphology and cross-section of the TiO₂ nanotube layer are illustrated in Figure 2. The nanotubes were densely packed and vertically oriented. The formation of a porous or nanotubular oxide layer on a metallic substrate is the result of three reactions: oxidation of the metallic surface of the substrate, dissolution of metal ions in the electrolyte, and selective chemical dissolution of the oxide layer caused by etching compounds (e.g., hydrofluoric acid HF) in the electrolyte [52]. The gap between the nanotubes was visible. The average inner diameter of the nanotubes was about 71 ± 7 nm and their average length was about 398 ± 11 nm, while the wall thickness was about 14 ± 2 nm. The wall thickness was uneven; this phenomenon may have been caused by voltage fluctuations in the oxidation process [53]. The bottom view images of the nanotubes (Figure 2d) show a dense barrier layer formed between the nanotubes and the titanium substrate. This type of nanotube oxide layer with comparable morphology was previously found on titanium while using orthophosphoric and hydrofluoric acid-based electrolytes [5,54]. By selecting oxidation parameters, it was possible to tune the dimensions of the resulting nanotubes [55]. It was proved that by using acidic electrolytes, the growth of nanotubes longer than 500 nm was not possible due to the high dissolution rate of the formed oxide layer [56]. The phenomena of pore formation and the selective dissolution of the TiO₂ oxide layer were attributed to the presence of fluoride ions in the electrolyte [57].
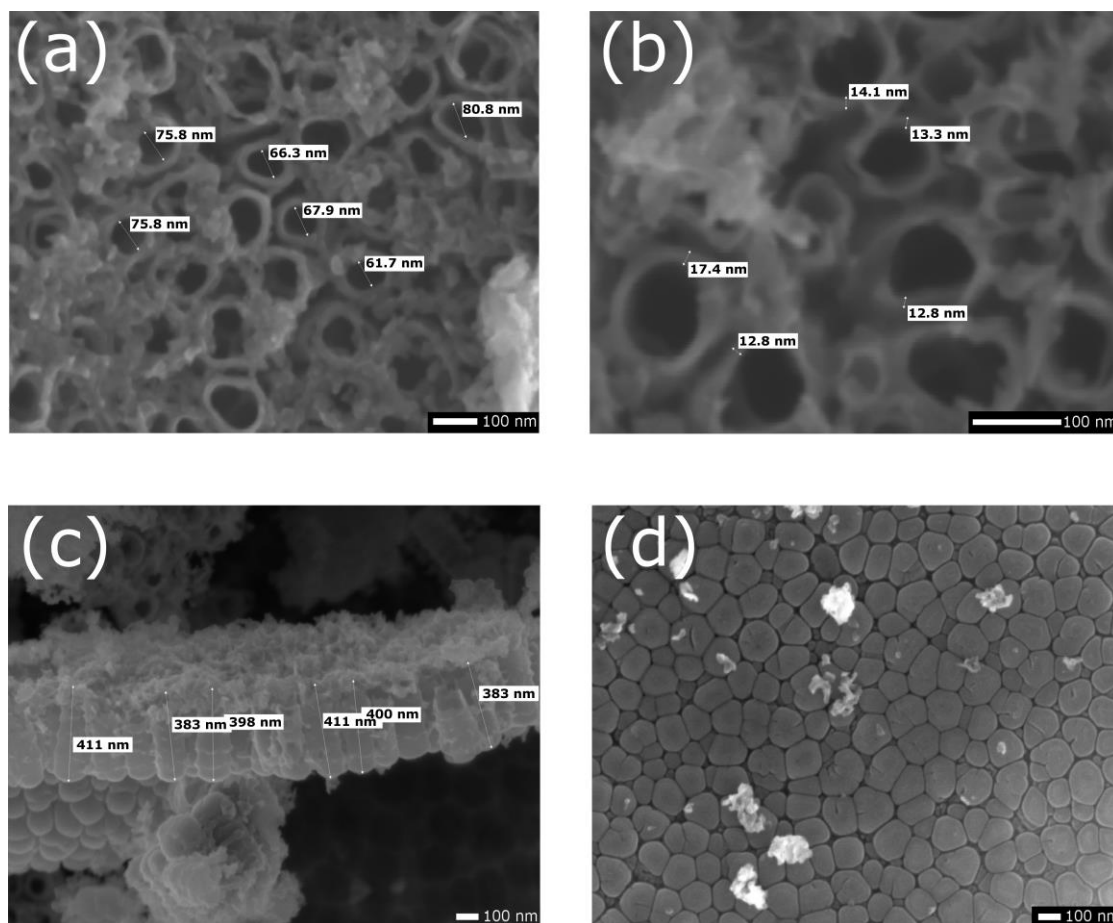

Figure 2. SEM images of TiO₂ nanotubes on titanium grade 2 obtained by electrochemical anodization at 20 V for 20 min: (**a**) top view with inner diameter measurements of nanotubes; (**b**) top view with nanotube wall thickness measurements; (**c**) cross-sectional view with nanotube length measurements; and (**d**) bottom view of nanotubes.

The morphology of chit/EE100 EPD coatings on the surface of pretreated Ti grade 2 is presented in Figure 3. All prepared coatings covered the titanium substrate completely, and there were no visible discontinuities in the coatings. Coatings deposited on a substrate

previously etched and subjected to electrochemical oxidation exhibited a more heterogeneous surface compared to coatings deposited on the ground surface. The morphology of the deposited coatings reflected the irregularities of the titanium surface after pretreatment. In all cases, the surface of the coatings revealed traces of hydrogen bubbles forming on the cathode during the EPD process. This phenomenon was less pronounced for coatings deposited on the etched surface, where the chit/EE100 coating embedded itself in the deeper irregularities of the etched surface of the titanium substrate. The unfavorable electrolysis of water during the EPD process, which significantly deteriorates the uniformity of the as-deposited coatings, could be mitigated by using another liquid medium to prepare the EPD suspension [58]. The effect of the applied chit/EE100 coating deposition parameters on their morphology was less clear. It can be noted that increasing the applied deposition voltage intensified the electrolysis of water and formation of more hydrogen bubbles on the cathode, which contributed to a more porous coating. The EPD mechanism of chitosan and Eudragit E 100 deposition is based on the positive charge of chitosan and Eudragit E 100 molecules because of their protonation in acetic acid solutions and formation of cationic electrolytes. The absorption of chitosan and Eudragit E 100 on the negatively charged cathode arises from the electrophoretic movement of the macromolecules of these biopolymers during EPD. As a result, the pH at the electrode surface increases and the positively charged biopolymer molecules are subsequently neutralized [47,59].
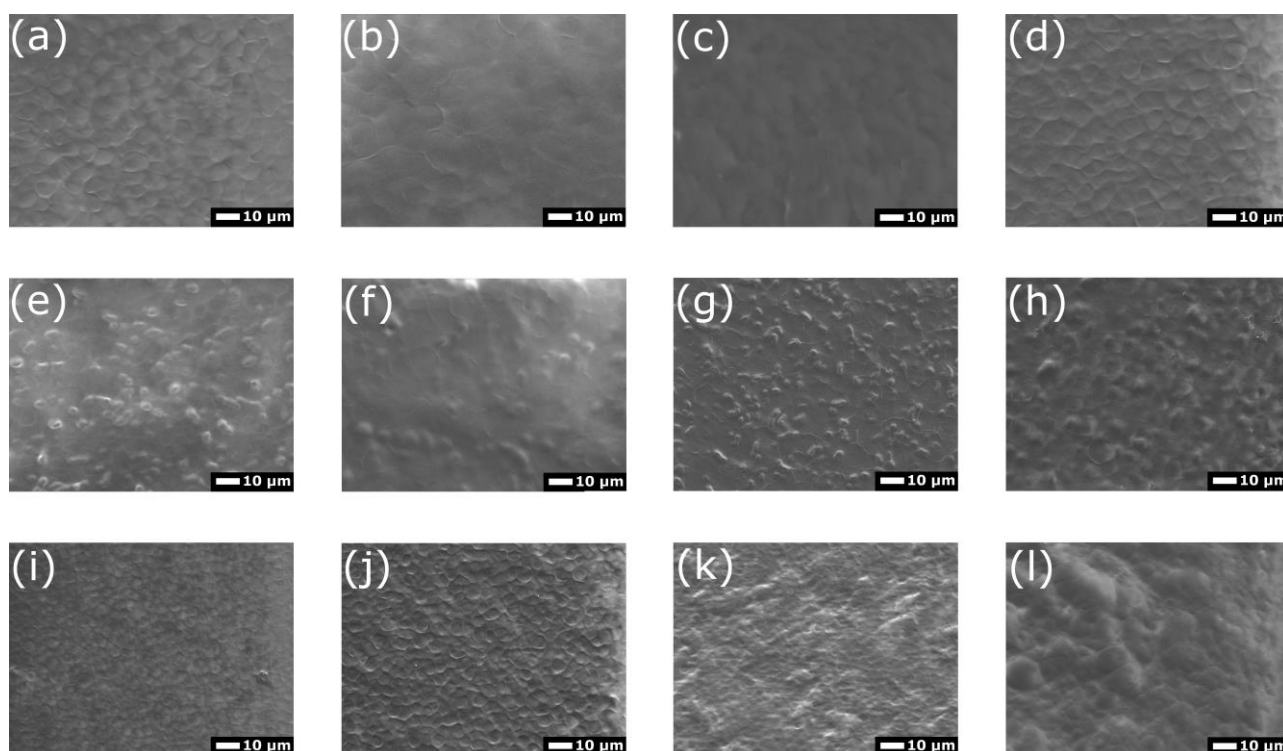

Figure 3. SEM images of chitosan/EE100 coatings deposited on the surface of pre-treated Ti grade 2 samples for different process parameters: (**a**) G1, (**b**) G2, (**c**) G1′, (**d**) G2′, (**e**) E1, (**f**) E2, (**g**) E1′, (**h**) E2′, (**i**) A1, (**j**) A2, (**k**) A1′, and (**l**) A2′ sample, magnification ×1000.

The atomic force microscopy 3D surface topography maps are depicted in Figure 4. To quantitatively describe the surface topography of the studied samples, the values of the arithmetic mean deviation (Sa), maximum peak height (Sp), and maximum valley depth (Sv) were determined, and the values are presented in Table 3. Among the selected surface pretreatment methods for the deposition of biopolymers, the surface roughness value of titanium grade 2 increased in the order G < A < E. As expected, the etching process of the titanium substrate contributed to a surface with the highest roughness. Deposition of the chit/EE100 biopolymer coating on the prepared surfaces resulted in a reduction in

the roughness of these surfaces, although the trend between the different types of surface preparation methods remained the same. This was most likely because of the particles of the deposited biopolymers filling the cavities created in the substrate by surface pretreatment and creating a smooth surface. The effect of the coating deposition parameters on the surface roughness value was less pronounced. For the E-series samples, it was determined that increasing deposition time and voltage contributed to a decrease in surface roughness. The increase in these deposition parameters resulted in more biopolymer particles' deposition and the filling of sizable irregularities after the etching process. In the case of long-term implant surfaces, the topography is the decisive factor of the correct osseointegration of the implant with bone tissue. The effect of roughness on the viability of osteogenic cells has been widely studied previously [60,61]. The positive effect of increased roughness on the adhesion of L929 fibroblasts and MG-63 osteoblasts has been proven [62]. Thus, in the present results, the most biocompatible coatings are the E group coatings. Conversely, it has been speculated that with the increase of roughness, the risk of bacterial biofilm formation also increases [63].

The results of the thickness measurements of the coatings deposited on the substrates prepared using various methods are presented in Table 3. Coatings deposited on a ground titanium substrate (group G) were characterized by the highest thickness. Lower thickness values of deposited coatings were observed for etched samples and were the lowest for samples after electrochemical oxidation. For all groups of samples, there was a tendency for the coating thickness to increase as the deposition time increased. This trend was not visible for the increasing deposition voltage. Most likely, the increase in the applied deposition voltage significantly increased the intensity of the water hydrolysis process, resulting in the more intense formation of hydrogen bubbles on the cathode, which contributed to an increase in the heterogeneity of the deposited film thickness distribution [64]. The fairly high standard deviations of the measured coating thickness values may be due to local non-uniformity of the produced coatings or the limited sensitivity of the measuring tool.
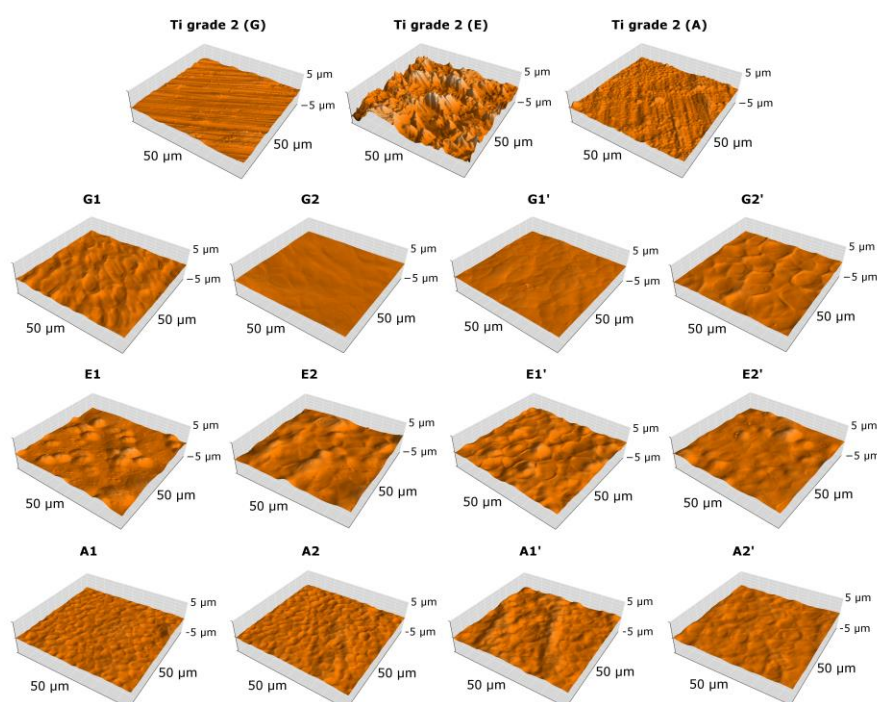

Figure 4. Surface topographies obtained by atomic force microscopy of the investigated samples.

Table 3. Surface topography parameters and coatings' thickness measurement results.

Sample	Surface Topography Parameters			Coating Thickness (μm)
	Sa (nm)	Sp (nm)	Sv (nm)	
Ti grade 2 (G)	128 ± 8	943 ± 291	−672 ± 195	–
Ti grade 2 (E)	582 ± 47	4458 ± 213	−2684 ± 178	–
Ti grade 2 (A)	157 ± 18	1232 ± 479	−591 ± 79	–
G1	111 ± 1	578 ± 25	−470 ± 55	2.86 ± 0.51
G2	75 ± 11	698 ± 202	−263 ± 59	6.24 ± 0.69
G1′	75 ± 1	464 ± 32	−299 ± 33	3.54 ± 0.97
G2′	106 ± 13	596 ± 178	−397 ± 17	6.45 ± 1.57
E1	272 ± 41	1765 ± 331	−1252 ± 226	2.19 ± 0.15
E2	251 ± 16	1364 ± 356	−1009 ± 120	2.29 ± 0.24
E1′	219 ± 12	1059 ± 95	−732 ± 56	1.66 ± 0.23
E2′	156 ± 25	1001 ± 254	−673 ± 156	2.60 ± 0.91
A1	96 ± 12	536 ± 114	−445 ± 133	1.46 ± 0.71
A2	103 ± 11	454 ± 47	−436 ± 53	2.14 ± 0.44
A1′	214 ± 6	770 ± 9	−679 ± 37	1.74 ± 0.39
A2′	145 ± 12	452 ± 41	−491 ± 81	1.84 ± 0.49

Qualitative EDS analysis of samples with chit/EE100 coatings deposited on the substrate after grinding, etching, and electrochemical oxidation (samples G1, E1, and A1, respectively) revealed characteristic peaks relating to the substrate material (Ti) and biopolymer coating (C, O, N) (Figure 5a,b,c). Peaks related to the sputtered chromium (Cr) layer were also visible. For G1 and A1 samples, a weak peak from silicon (Si) was also identified, most likely resulting from the grinding process of the samples at the surface preparation stage for coating deposition.

The FTIR analysis results are given in Figure 5d. G2, E2, and A2 samples were selected for testing due to the increased thickness of the chit/EE100 coatings. Intensities related to both chitosan and Eudragit E 100 were identifiable on the spectra [65,66]. At 2940 cm^{-1}, 1450 cm^{-1}, and 1380 cm^{-1}, the vibrations of the CH_x groups of Eudragit E 100 were distinguishable. The absorptions at 2865 cm^{-1} and 2820 cm^{-1}, in turn, could be attributed to the dimethylamine groups of EE100. A strong C=O ester stretching band at 1750 cm^{-1} was detected. Other typical bands for EE100 ester groups were observed in the 1300–1145 cm^{-1} range. Concerning chitosan [66], oscillations of carbonyl bonds (C=O) from amide groups in the range of 1650–1450 cm^{-1} were reported. CO bond vibrations could be identified from the absorption between 1145 and 1000 cm^{-1}. The results confirmed that the produced coatings are a blend of chitosan and Eudragit E 100.
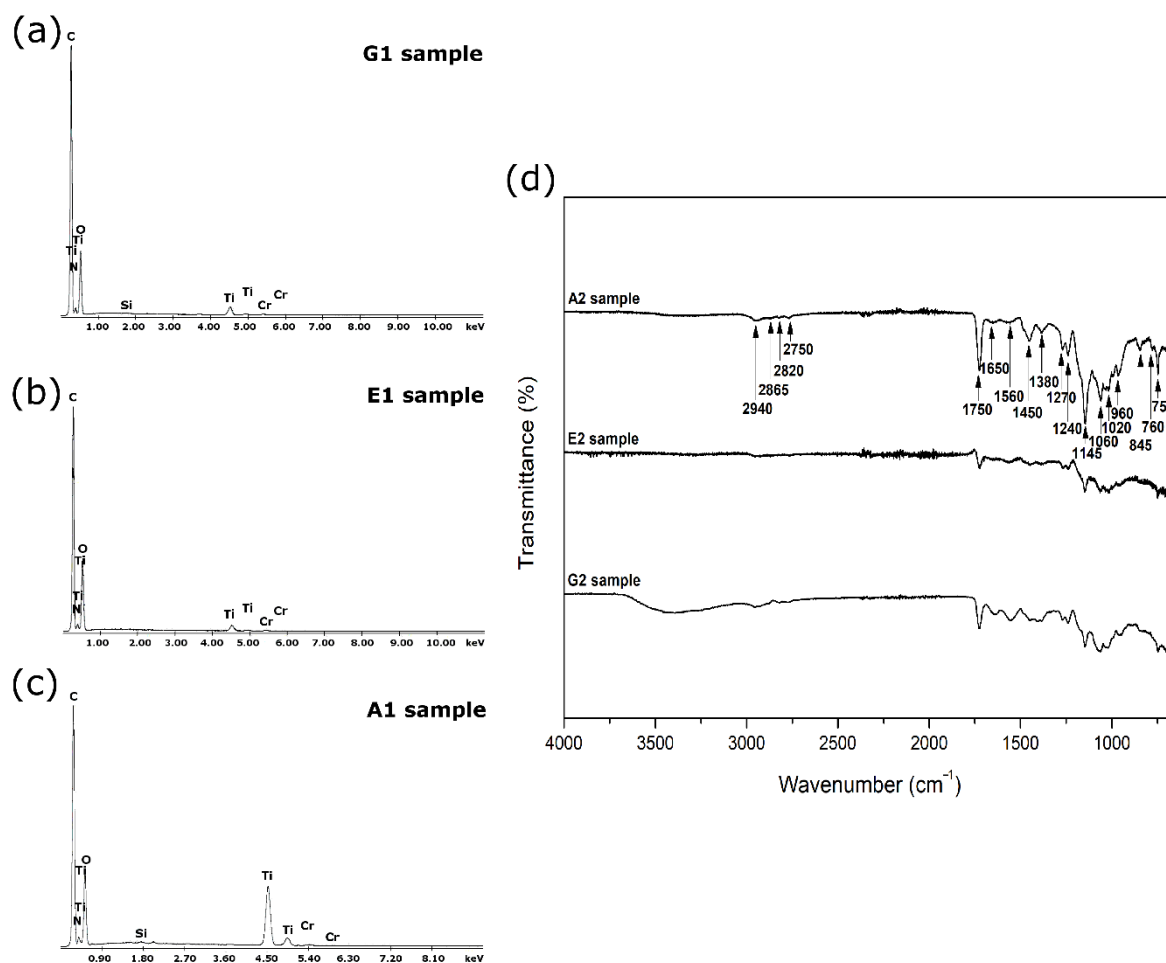
Figure 5. EDS (**a**), (**b**), (**c**), and FTIR (**d**) analysis results of samples with chit/EE100 coatings deposited on substrates after (**a**) grinding (sample G1), (**b**) etching (sample E1), and (**c**) electrochemical oxidation (sample A1).

3.2. Wettability Study

The results of the contact angle measurements of titanium substrates and samples with biopolymer coatings are depicted in Figure 6. Except for the sample Ti grade 2 (E), all other specimens were characterized as hydrophilic but with still relatively high contact angle values. Among the samples without coatings, the contact angle value followed the trend G < A < E, similar to the results of the roughness measurements of these surfaces. The lowest contact angle value was determined for the titanium substrate after grinding (sample G). Among the coated samples, the G-series samples showed relatively better wettability. The effect of the applied chit/EE100 coating deposition parameter on the wetting angle value of the produced coating was scarcely evident. The results generated for the chit/EE100 coatings were similar to those reported in the previous study [47]. In comparing the results of the contact angle measurements with the surface roughness measurements of the prepared samples, for most samples, a trend was evident: as the surface roughness increased, the value of the contact angle also increased.

Currently, the possibility of modifying and controlling the surface wettability of biomaterials has drawn considerable scientific and technological interest. There are reports about the increased wettability of the implant surface, which improves its biocompatibility [67]. In biological systems, implant wettability plays a crucial role in mediating protein adsorption and cell adhesion; however, this also refers to bacterial cells [7,68]. The literature data indicate that an increase in the hydrophobicity of the biomaterial surface contributes to a reduction in bacterial adhesion [69]. It is, therefore, necessary to obtain a sur-

face with optimum wettability that will provide easy adhesion of, for example, bone-forming cells and at the same time be less susceptible to bacterial colonization. For bone cells, an optimal contact angle value that provides the best cell proliferation is assumed to be 35–85°, with an optimal value of 55° [70]. The coated samples produced in this study were within this range. Additionally, to reduce bacterial adhesion without significantly changing the wettability of the surface, the produced coatings could be enriched with substances with antimicrobial activity, e.g., silver or copper nanoparticles [71].
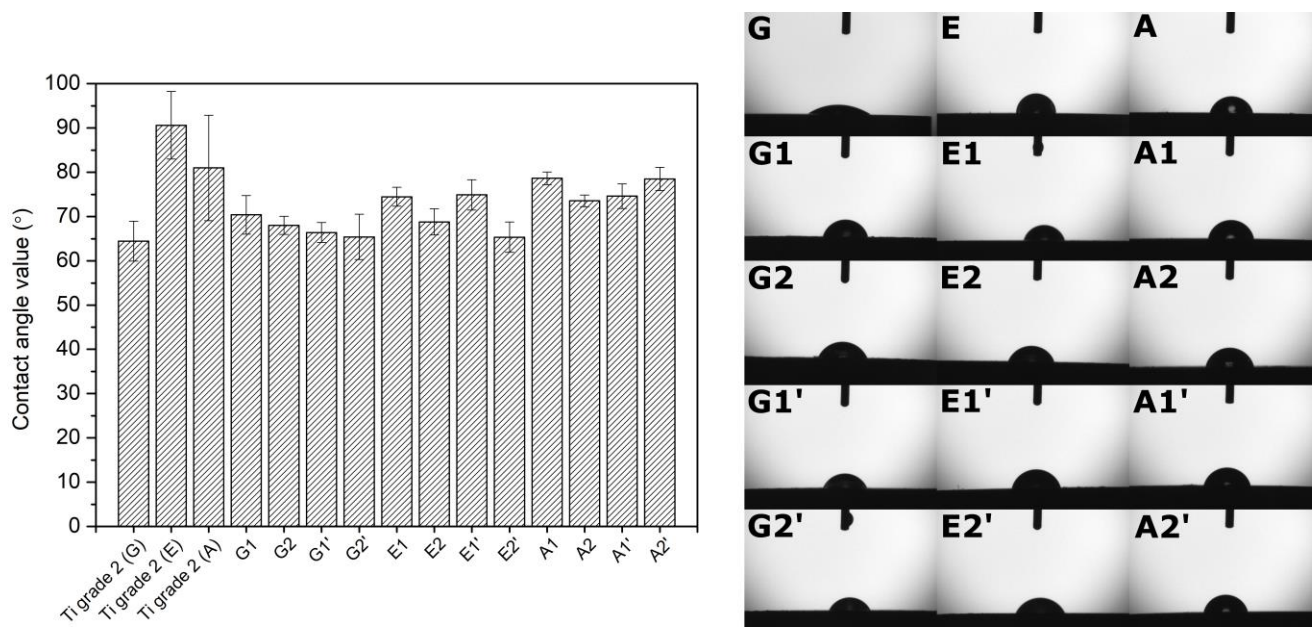

Figure 6. The results of the water contact angle measurements for the surface of pre-treated Ti grade 2 substrates and the modified substrates with chit/EE100 coatings obtained for different process parameters. Data are presented as the mean ± SD (n = 5).

3.3. Adhesion Study

Selected critical force versus friction force relationship curves and the corresponding microscopic images of single scratches with marked critical force (Lc) causing the complete removal of the biopolymer coating from the metallic substrate obtained from the scratch test are shown in Figure 7. The average critical load and critical friction force values calculated from ten scratches are summarized in Table 4.

The area of complete biopolymer coating removal from the titanium substrate prepared before deposition was determined by the abrupt change in the value of the indenter friction force on the metal substrate. The values corresponded to the scratch images from the optical microscope. The higher Lc force value reflected better adhesion of the chit/EE100 coating to the titanium substrate. Based on the results obtained, the best adhesion to a properly prepared metallic substrate was observed for the coatings deposited on the substrate after electrochemical oxidation (series A). However, those Lc values were comparable to those for coatings deposited on previously ground titanium (series G). For the etched samples (series E), it was difficult to determine the exact location of coating delamination because the surface of these samples possessed the highest inhomogeneity and individual scratches were barely visible. The effect of the applied EPD parameters of coating deposition on the adhesion of the coatings to the substrate was negligible. Concerning surface roughness, a higher adhesion of the coating to the metallic substrate was observed for the less rough substrate. The research study determined the positive effect of electrochemical oxidation on the adhesion of biopolymer coatings. Similar results are observed from the tests for other coatings deposited on the titanium alloy [72,73]. For coatings deposited on a TiO_2 nanotube substrate, the improvement in adhesion can be

attributed to the increase in the surface area caused by surface modification at the nanoscale. In addition, increased adhesion should be attributed to the C=O bond between the coating and nanotube substrate, where the highest band intensity in the FTIR test was confirmed for coatings of group A. Tests of biopolymer coatings deposited by the electrophoretic method are not frequently performed; however, the adhesion tests of such coatings are crucial for determining their mechanical properties. Tests with the use of the scratch-test technique for biocomposite EPD coatings (chitosan/gelatin/silica-gentamicin/bioactive glass) showed values of the critical force at the level of no more than 30 mN, with a maximum set force of 500 mN [74].
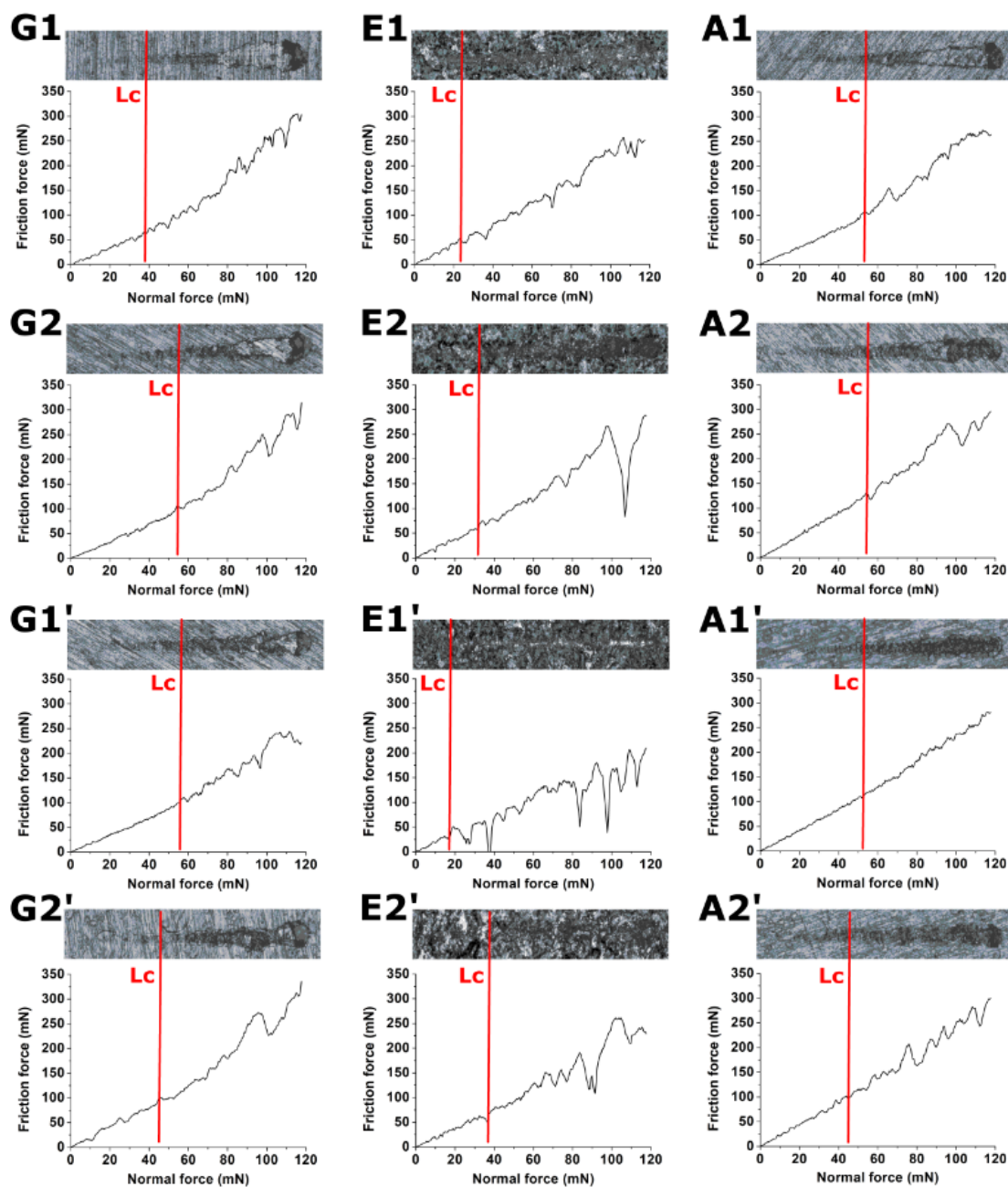

Figure 7. Scratch test curves obtained for coated specimens along with a single-scratch image and marked critical load value (Lc).

Table 4. The critical load and critical friction values determined from the scratch test of chit/EE100 coatings deposited on substrates prepared variously.

Sample	Critical Load (mN)	Critical Friction (mN)
G1	37.63 ± 4.63	55.56 ± 8.28
G2	57.18 ± 4.22	97.77 ± 9.94
G1′	55.84 ± 2.12	97.91 ± 5.96
G2′	43.54 ± 6.48	90.46 ± 17.18
E1	23.29 ± 4.67	44.85 ± 12.06
E2	31.91 ± 4.42	59.40 ± 10.55
E1′	19.53 ± 5.17	35.98 ± 11.60
E2′	34.11 ± 7.24	59.32 ± 13.16
A1	53.31 ± 4.41	100.19 ± 10.65
A2	54.15 ± 8.31	123.11 ± 22.05
A1′	52.07 ± 5.89	117.52 ± 14.69
A2′	44.82 ± 4.54	104.10 ± 14.00

3.4. Corrosion Studies

The results of the electrochemical assay are presented in Figure 8 and Table 5. The OCP value was used as a parameter to determine the initial corrosion resistance of the tested samples. All samples achieved stabilization in the SBF solution after 1 h (Figure 8a). An increase in the OCP value over time was observed for all tested samples because of the progressive stabilization of the forming passive layer; however, the course of the curves was moderate [75]. For coated samples, the open circuit potential values were shifted towards positive values as compared to samples without coatings. The recorded OCP values were in the range of about −0.4 to 0.1 V. The most positive value of the potential was recorded for the G1 sample.

The OCP value corresponded to the approximate value of E_{corr}. According to the corrosion curves (Figure 8b), the E_{corr} values of coated samples were higher compared to a bare sample, demonstrating lower corrosion resistance, and OCP values also shifted into less noble potentials. Based on the curves, corrosion parameters were determined using the Tafel extrapolation method (Table 5). The highest E_{corr} value was recorded for sample G1. However, the i_{corr} values for all samples were relatively low, on the order of nA/cm^2. Similar results were obtained in previous studies of samples made of titanium or its alloys [47,71]. The formation of an oxide nanotube layer on the titanium grade 2 surface ensured higher corrosion resistance of the sample compared to the other two types of surface pretreatments. Presumably, the nanotube oxide layer provided a barrier separating the metallic substrate from the corrosive environment (as shown in Figure 2d), resulting in higher corrosion resistance [76]. Deposition of the biopolymer coating on modified substrates contributed to a decrease in the corrosion resistance of the samples. This is most likely due to the coatings' non-uniformity, which may contribute to the formation of corrosion channels [77]. In comparing the values of Tafel slopes, for the samples without coatings, the β_c value was lower than the β_a value. This indicates that anodic processes are faster than cathodic processes in this system. The higher the value of the R_{pol} resistance, the smaller the corrosion rate, thus the corrosion resistance of the coating can be evaluated by the R_{pol} value. Significantly higher R_{pol} values were observed for samples without coatings, which corresponded to a lower i_{corr} value [78].

Figure 8c,d present the EIS data. The Nyquist plots were well-defined at high and low frequencies. The impedance was characterized by employing a quarter-circle capacitive loop for all samples. Similar shapes of impedance curves were reported in other studies on chitosan-based coatings [79]. The E-series samples exhibited the highest impedance, while the ground samples exhibited the lowest values. The correlations between the uncoated samples and samples with chit/EE100 coatings were merely visible. In analyzing

the Bode-phase diagrams in Figure 8d, the phase angles for all samples approached 0° at high frequencies, suggesting that the impedance was mainly dominated by the electrolyte resistance [79]. At lower frequencies, the phase angles of the uncoated and coated sample after etching were higher than those of the other samples. According to the Bode plots, within the whole frequency range, the samples showed higher impedance after electrochemical oxidation, which indicated higher corrosion resistance. The results did not completely coincide with the corrosion curves, which may be due to the changing test conditions. The corrosion curves were measured after the impedance tests, thus the prolonged presence of the samples in the SBF solution could contribute to the swelling of the biopolymer coating, which could have affected the corrosion resistance of the tested sample [71].

Figure 9 depicts the microstructure of the samples after electrochemical testing. For both pretreated samples and coated specimens, no evidence of corrosion impact was evident. As in previous studies, when exposed to the SBF environment, swelling of the biopolymer coating was visible in the SEM images. Swelling occurs due to an increase in the volume of the polymer as a result of solvent uptake. This mechanism is often considered in biopolymer coatings [80].
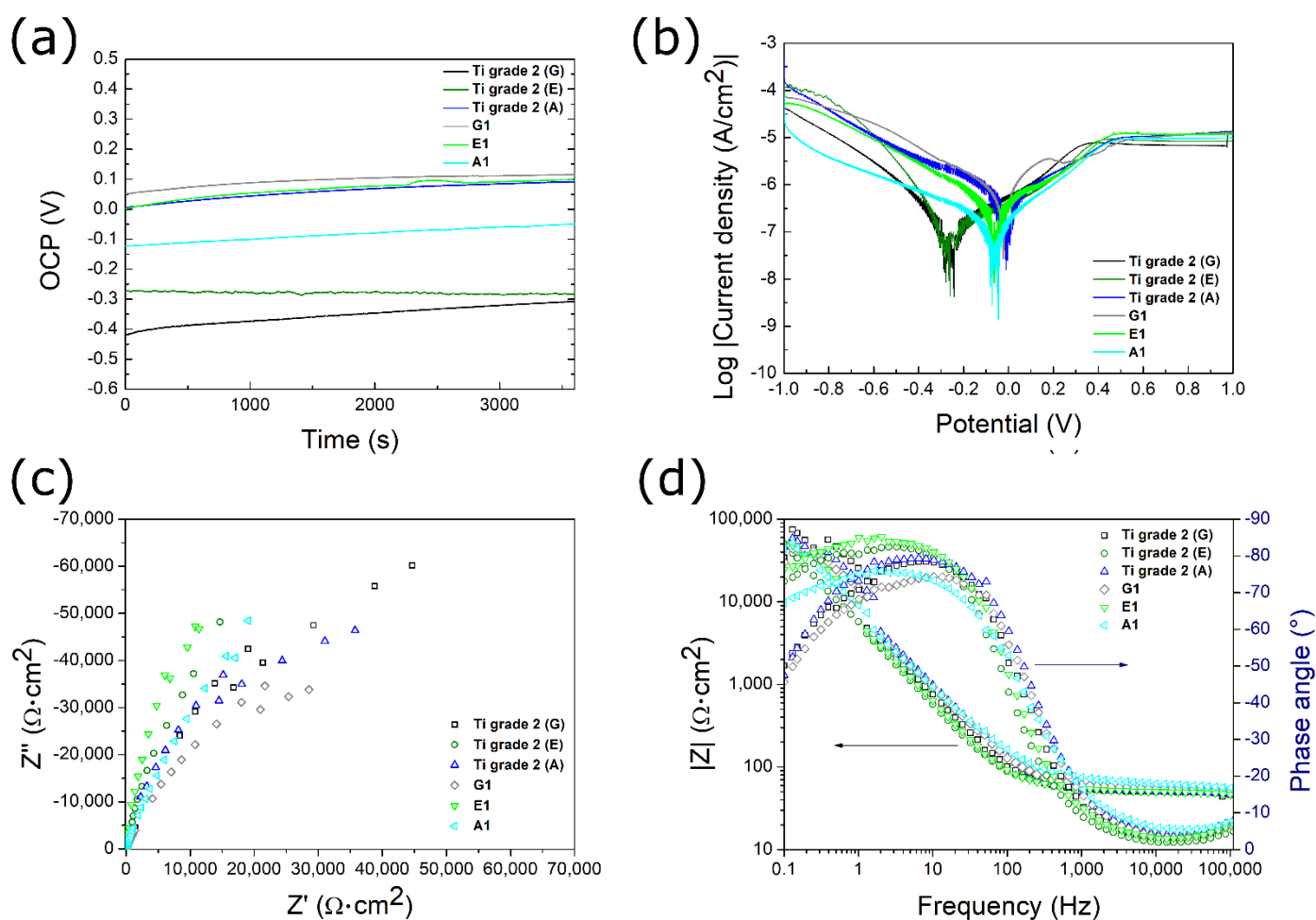

Figure 8. (**a**) Open circuit potential (OCP); (**b**) potentiodynamic polarization curves; (**c**) Nyquist plots; and (**d**) Bode plots of the surface of pre-treated Ti grade 2 substrates and samples with chit/EE100 coatings.

Table 5. Open circuit potential (OCP); corrosion potential (E_{corr}); current density (i_{corr}); Tafel slope values (β_a and β_c); and polarization resistance (R_{pol}) of the investigated samples.

Sample	OCP (V)	E_{corr} (V)	i_{corr} (nA/cm²)	β_a (mV)	β_c (mV)	R_{pol} (kΩ·cm²)
Ti grade 2 (G)	−0.307	−0.234	84.905	314.318	219.406	660.804
Ti grade 2 (E)	−0.282	−0.257	101.973	423.702	159.648	493.759
Ti grade 2 (A)	−0.376	−0.340	64.237	513.015	113.258	627.128
G1	0.115	−0.041	654.635	175.330	370.191	78.918
E1	0.097	−0.065	393.674	446.942	379.676	226.428
A1	−0.049	−0.062	190.636	327.120	568.025	472.877
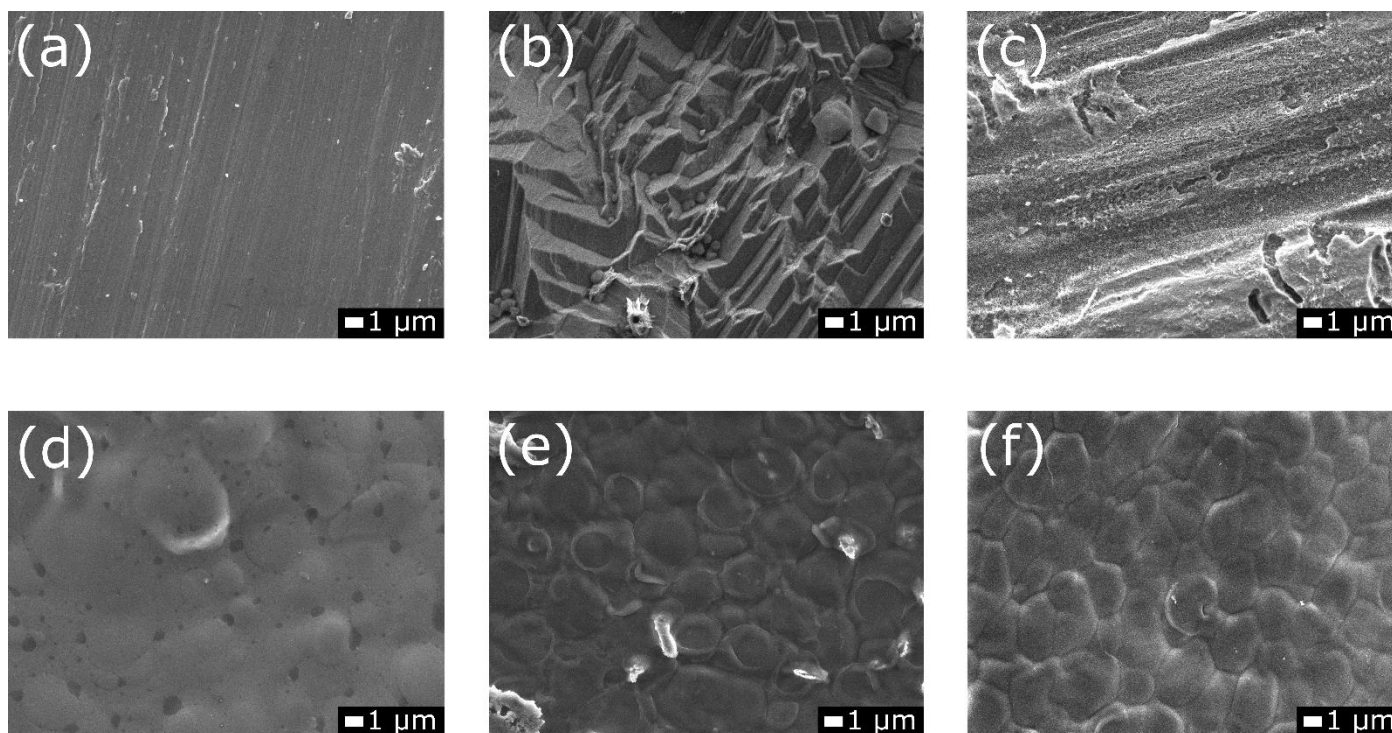
Figure 9. SEM images of the surface of pre-treated Ti grade 2 substrates after (**a**) wet grinding (G), (**b**) acid etching (E), and (**c**) electrochemical anodization (A), and for the samples: (**d**) G1, (**e**) E1, and (**f**) A1 with chit/EE100 coatings after electrochemical tests (images obtained with magnification at ×5000).

4. Conclusions

Surface modifications of metallic biomaterials significantly affects their physicochemical properties. It is difficult to determine which of the proposed techniques for substrate preparation, before the deposition of biopolymer coatings, grinding, etching, or electrochemical oxidation, results in the best coating performance. However, based on the performed tests, it can be concluded that the coatings deposited on the nanotube oxide substrate showed high uniformity, adequate thickness (about 1.8 μm) and roughness (Sa about 140 nm), satisfactory wettability (θ ≈ 75°), and the highest adhesion (Lc value around 50 mN) to the metallic substrate in comparison with the other coatings deposited on substrates prepared differently. In addition, these samples showed superior corrosion resistance in an environment simulating human body fluids, which is particularly important for implant applications. Besides the biopolymer coating, the nanotube oxide layers additionally separated the metallic substrates from the corrosive medium. Such layers can provide an excellent carrier for the drug substance, which, in combination with a smart biopolymer coating based on chitosan and Eudragit E 100, will enable the development of a controlled drug delivery system. The applied EPD process parameters changed

the morphology of the coatings, which translated into changes in the surface roughness and wettability. Their effect on adhesion and corrosion resistance is less pronounced.

References

1. Casagrande, R.B.; Kunst, S.R.; Beltrami, L.V.R.; Aguzzoli, C.; Brandalise, R.N.; de Fraga Malfatti, C. Pretreatment effect of the pure titanium surface on hybrid coating adhesion based on tetraethoxysilane and methyltriethoxysilane. *J. Coat. Technol. Res.* **2018**, *15*, 1089–1106.
2. Chouirfa, H.; Bouloussa, H.; Migonney, V.; Falentin-Daudré, C. Review of titanium surface modification techniques and coatings for antibacterial applications. *Acta Biomater.* **2019**, *83*, 37–54.
3. Kaur, M.; Singh, K. Review on titanium and titanium based alloys as biomaterials for orthopaedic applications. *Mater. Sci. Eng. C* **2019**, *102*, 844–862.
4. Spriano, S.; Yamaguchi, S.; Baino, F.; Ferraris, S. A critical review of multifunctional titanium surfaces: New frontiers for improving osseointegration and host response, avoiding bacteria contamination. *Acta Biomater.* **2018**, *79*, 1–22.
5. Bartmański, M.; Pawłowski, Ł.; Zieliński, A.; Mielewczyk-Gryń, A.; Strugała, G.; Cieslik, B. Electrophoretic deposition and characteristics of chitosan / nanosilver composite coatings on the nanotubular TiO_2 layer. *Coatings* **2020**, *10*, 245.
6. Doe, Y.; Ida, H.; Seiryu, M.; Deguchi, T.; Takeshita, N.; Sasaki, S.; Sasaki, S.; Irie, D.; Tsuru, K.; Ishikawa, K.; et al. Titanium surface treatment by calcium modification with acid-etching promotes osteogenic activity and stability of dental implants. *Materialia* **2020**, *12*, 100801.
7. Lin, Z.; Wang, Y.; Wang, D. ning; Zhao, B. hong; Li, J. chang Porous structure preparation and wettability control on titanium implant. *Surf. Coat. Technol.* **2013**, *228*, S131–S136.
8. Manivasagam, G.; Dhinasekaran, D.; Rajamanickam, A. Biomedical Implants: Corrosion and its Prevention-A Review Surface modification of Ti alloys by plasma cleaning to enhance antibacterial activity-BRNS View project Biomedical Implants: Corrosion and its Prevention-A Review. *Recent Pat. Corros. Sci.* **2010**, *2*, 40–54.
9. Tolde, Z.; Starý, V.; Cvrček, L.; Vandrovcová, M.; Remsa, J.; Daniš, S.; Krčil, J.; Bačáková, L.; Špatenka, P. Growth of a TiNb adhesion interlayer for bioactive coatings. *Mater. Sci. Eng. C* **2017**, *80*, 652–658.
10. Lackner, J.M.; Waldhauser, W.; Schwarz, M.; Mahoney, L.; Major, L.; Major, B. Polymer pre-treatment by linear anode layer source plasma for adhesion improvement of sputtered TiN coatings. *Vacuum* **2008**, *83*, 302–307.
11. Ergün, Y.; Başpınar, M.S. Effect of acid passivation and H_2 sputtering pretreatments on the adhesive strength of sol–gel derived Hydroxyapatite coating on titanium surface. *Int. J. Hydrog. Energy* **2017**, *42*, 20420–20429.
12. Sasikumar, Y.; Indira, K.; Rajendran, N. Surface Modification Methods for Titanium and Its Alloys and Their Corrosion Behavior in Biological Environment: A Review. *J. Bio-Tribo-Corros.* **2019**, *5*, 1–25.
13. Man, H.C.; Chiu, K.Y.; Cheng, F.T.; Wong, K.H. Adhesion study of pulsed laser deposited hydroxyapatite coating on laser surface nitrided titanium. *Thin Solid Film.* **2009**, *517*, 5496–5501.
14. Soro, N.; Saintier, N.; Attar, H.; Dargusch, M.S. Surface and morphological modification of selectively laser melted titanium lattices using a chemical post treatment. *Surf. Coat. Technol.* **2020**, *393*, 125794.
15. Basiaga, M.; Walke, W.; Antonowicz, M.; Kajzer, W.; Szewczenko, J.; Domanowska, A.; Michalewicz, A.; Szindler, M.; Staszuk, M.; Czajkowski, M. Impact of surface treatment on the functional properties stainless steel for biomedical applications. *Materials* **2020**, *13*, 1–17.
16. Iwaya, Y.; Machigashira, M.; Kanbara, K.; Miyamoto, M.; Noguchi, K.; Izumi, Y.; Ban, S. Surface Properties and Biocompatibility of Acid-etched Titanium. *Dent. Mater. J.* **2008**, *27*, 415–421.

17. Ren, B.; Wan, Y.; Wang, G.; Liu, Z.; Huang, Y.; Wang, H. Morphologically modified surface with hierarchical micro-/nano-structures for enhanced bioactivity of titanium implants. *J. Mater. Sci.* **2018**, *53*, 12679–12691.

18. Yang, G.L.; He, F.M.; Yang, X.F.; Wang, X.X. Zhao, S.F. Bone responses to titanium implants surface-roughened by sandblasted and double etched treatments in a rabbit model. *Oral Surg. Oral Med. Oral Pathol. Oral Radiol. Endodontology* **2008**, *106*, 516–524.

19. de Lima, G.G.; da Luz, A.R.; Pereira, B.L.; Szesz, E.M.; de Souza, G.B.; Lepienski, C.M.; Kuromoto, N.K.; Nugent, M.J.D. Tailoring surface properties from nanotubes and anodic layers of titanium for biomedical applications. In *Applications of Nanocomposite Materials in Orthopedics*; Elsevier: Amsterdam, The Netherlands, 2018; pp. 179–199, ISBN 9780128137574.

20. Jiang, T.; Zhang, Z.; Zhou, Y.; Liu, Y.; Wang, Z.; Tong, H.; Shen, X.; Wang, Y. Surface functionalization of titanium with chitosan/gelatin via electrophoretic deposition: Characterization and cell behavior. *Biomacromolecules* **2010**, *11*, 1254–1260.

21. Bartmanski, M.; Cieslik, B.; Glodowska, J.; Kalka, P.; Pawlowski, L.; Pieper, M.; Zielinski, A. Electrophoretic deposition (EPD) of nanohydroxyapatite—Nanosilver coatings on Ti13Zr13Nb alloy. *Ceram. Int.* **2017**, *43*, 11820–11829.

22. Cheung, K.H.; Pabbruwe, M.B.; Chen, W.F.; Koshy, P.; Sorrell, C.C. Effects of substrate preparation on TiO2 morphology and topography during anodization of biomedical Ti6Al4V. *Mater. Chem. Phys.* **2020**, *252*, 123224.

23. Nicoli, L.G.; de Oliveira, G.J.P.L.; Lopes, B.M.V.; Marcantonio, C.; Zandim-Barcelos, D.L.; Marcantonio, E. Survival/success of dental implants with acid—Etched surfaces: A retrospective evaluation after 8 to 10 years. *Braz. Dent. J.* **2017**, *28*, 330–336.

24. Szmukler-Moncler, S.; Bischof, M.; Nedir, R.; Ermrich, M. Titanium hydride and hydrogen concentration in acid-etched commercially pure titanium and titanium alloy implants: A comparative analysis of five implant systems. *Clin. Oral Implant. Res.* **2010**, *21*, 944–950.

25. Zhao, G.; Schwartz, Z.; Wieland, M.; Rupp, F.; Geis-Gerstorfer, J.; Cochran, D.L.; Boyan, B.D. High surface energy enhances cell response to titanium substrate microstructure. *J. Biomed. Mater. Res. Part A* **2005**, *74*, 49–58.

26. Matos, G.R.M. Surface Roughness of Dental Implant and Osseointegration. *J. Maxillofac. Oral Surg.* **2021**, *20*, 1–4.

27. Lim, Y.C.; Zainal, Z.; Tan, W.T.; Hussein, M.Z. Anodization parameters influencing the growth of titania nanotubes and their photoelectrochemical response. *Int. J. Photoenergy* **2012**, *2012*, doi:10.1155/2012/638017.

28. Lü, W.L.; Wang, N.; Gao, P.; Li, C.Y.; Zhao, H.S.; Zhang, Z.T. Effects of anodic titanium dioxide nanotubes of different diameters on macrophage secretion and expression of cytokines and chemokines. *Cell Prolif.* **2015**, *48*, 95–104.

29. Oh, S.; Jin, S. Titanium oxide nanotubes with controlled morphology for enhanced bone growth. *Mater. Sci. Eng. C* **2006**, *26*, 1301–1306.

30. Coelho, L.C.B.B.; Correia, M.T.S.; Silva, G.M.M.; Arruda, I.R.S.; Oliveira, W.F.; Machado, G. Functionalization of titanium dioxide nanotubes with biomolecules for biomedical applications. *Mater. Sci. Eng. C* **2017**, *81*, 597–606.

31. Çelik, I.; Alsaran, A.; Purcek, G. Effect of different surface oxidation treatments on structural, mechanical and tribological properties of ultrafine-grained titanium. *Surf. Coat. Technol.* **2014**, *258*, 842–848.

32. Lin, Z.; Li, S.J.; Sun, F.; Ba, D.C.; Li, X.C. Surface characteristics of a dental implant modified by low energy oxygen ion implantation. *Surf. Coat. Technol.* **2019**, *365*, 208–213.

33. Du Plooy, R.; Akinlabi, E.T. Analysis of laser cladding of Titanium alloy. In *Materials Today: Proceedings*; Elsevier: Amsterdam, The Netherlands, 2018; Volume 5, pp. 19594–19603.

34. Sharma, V.; Prakash, U.; Kumar, B.V.M. Surface composites by friction stir processing: A review. *J. Mater. Process. Technol.* **2015**, *224*, 117–134.

35. Liu, W.; Liu, S.; Wang, L. Surface Modification of Biomedical Titanium Alloy: Micromorphology, Microstructure Evolution and Biomedical Applications. *Coatings* **2019**, *9*, 249.

36. Morshed, M.M.; Cameron, D.C.; McNamara, B.P.; Hashmi, M.S.J. Pre-treatment of substrates for improved adhesion of diamond-like carbon films on surgically implantable metals deposited by saddle field neutral beam source. *Surf. Coat. Technol.* **2003**, *174–175*, 579–583.

37. Shum, P.W.; Zhou, Z.F.; Li, K.Y. Enhancement of adhesion strength and tribological performance of pure carbon coatings on Ti-6Al-4V biomaterials with ion implantation pre-treatments. *Tribol. Int.* **2007**, *40*, 313–318.

38. Eliaz, N.; Ritman-Hertz, O.; Aronov, D.; Weinberg, E.; Shenhar, Y.; Rosenman, G.; Weinreb, M.; Ron, E. The effect of surface treatments on the adhesion of electrochemically deposited hydroxyapatite coating to titanium and on its interaction with cells and bacteria. *J. Mater. Sci. Mater. Med.* **2011**, *22*, 1741–1752.

39. Ágata de Sena, L.; Calixto de Andrade, M.; Malta Rossi, A.; de Almeida Soares, G. Hydroxyapatite deposition by electrophoresis on titanium sheets with different surface finishing. *J. Biomed. Mater. Res.* **2002**, *60*, 1–7.

40. Kar, A.; Raja, K.S.; Misra, M. Electrodeposition of hydroxyapatite onto nanotubular TiO2 for implant applications. *Surf. Coat. Technol.* **2006**, *201*, 3723–3731.

41. Hallmann, L.; Mehl, A.; Sereno, N.; Hämmerle, C.H.F. The improvement of adhesive properties of PEEK through different pretreatments. *Appl. Surf. Sci.* **2012**, *258*, 7213–7218.

42. Kumaravel, V.; Nair, K.M.; Mathew, S.; Bartlett, J.; Kennedy, J.E.; Manning, H.G.; Whelan, B.J.; Leyland, N.S.; Pillai, S.C. Antimicrobial TiO2 nanocomposite coatings for surfaces, dental and orthopaedic implants. *Chem. Eng. J.* **2021**, *416*, 129071.

43. Wieszczycka, K.; Staszak, K.; Woźniak-Budych, M.J.; Litowczenko, J.; Maciejewska, B.M.; Jurga, S. Surface functionalization—The way for advanced applications of smart materials. *Coord. Chem. Rev.* **2021**, *436*, 213846.

44. Yuan, Z.; He, Y.; Lin, C.; Liu, P.; Cai, K. Antibacterial surface design of biomedical titanium materials for orthopedic applications. *J. Mater. Sci. Technol.* **2021**, *78*, 51–67.

45. Schmaljohann, D. Thermo- and pH-responsive polymers in drug delivery. *Adv. Drug Deliv. Rev.* **2006**, *58*, 1655–1670.

46. Pawłowski, Ł. pH-dependent composite coatings for controlled drug delivery system—Review. *Inżynieria Mater.* **2019**, *1*, 4–9.

47. Pawłowski, Ł.; Bartmański, M.; Strugała, G.; Mielewczyk-Gryń, A.; Jażdżewska, M.; Zieliński, A. Electrophoretic Deposition and Characterization of Chitosan/Eudragit E 100 Coatings on Titanium Substrate. *Coatings* **2020**, *10*, 607.

48. Loch, J.; Krawiec, H. Corrosion behaviour of cobalt alloys in artifical salvia solution. *Arch. Foundry Eng.* **2013**, *13*, 101–106.

49. Lim, H.S.; Hwang, M.J.; Jeong, H.N.; Lee, W.Y.; Song, H.J.; Park, Y.J. Evaluation of surface mechanical properties and grindability of binary Ti alloys containing 5 wt % Al, Cr, Sn, and V. *Metals* **2017**, *7*, 1–11.

50. Hung, K.Y.; Lin, Y.C.; Feng, H.P. The effects of acid etching on the nanomorphological surface characteristics and activation energy of titanium medical materials. *Materials* **2017**, *10*, 1164.

51. Li, H.; Chen, Z.; Zhao, A.Z.; Wang, Y.; Sun, H.; Lai, Y. TiO₂ nanotube platforms for smart drug delivery: A review. **2016**, *11*, 4819–4834.

52. Cipriano, A.F.; Miller, C.; Liu, H. Anodic growth and biomedical applications of TiO2 nanotubes. *J. Biomed. Nanotechnol.* **2014**, *10*, 2977–3003.

53. Tsuchiya, H.; Macak, J.M.; Taveira, L.; Balaur, E.; Ghicov, A.; Sirotna, K.; Schmuki, P. Self-organized TiO₂ nanotubes prepared in ammonium fluoride containing acetic acid electrolytes. *Electrochem. Commun.* **2005**, *7*, 576–580.

54. Kodama, A.; Bauer, S.; Komatsu, A.; Asoh, H.; Ono, S.; Schmuki, P. Bioactivation of titanium surfaces using coatings of TiO₂ nanotubes rapidly pre-loaded with synthetic hydroxyapatite. *Acta Biomater.* **2009**, *5*, 2322–2330.

55. Poddar, S.; Bit, A.; Sinha, S.K. A study on influence of anodization on the morphology of titania nanotubes over Ti6Al4V alloy in correlation to hard tissue engineering application. *Mater. Chem. Phys.* **2020**, *254*, 123457.

56. Varghese, O.K.; Gong, D.; Paulose, M.; Grimes, C.A.; Dickey, E.C. Crystallization and high-temperature structural stability of titanium oxide nanotube arrays. *J. Mater. Res.* **2003**, *18*, 156–165.

57. Prakasam, H.E.; Shankar, K.; Paulose, M.; Varghese, O.K.; Grimes, C.A. A new benchmark for TiO₂ nanotube array growth by anodization. *J. Phys. Chem. C* **2007**, *111*, 7235–7241.

58. Sorkhi, L.; Farrokhi-Rad, M.; Shahrabi, T. Electrophoretic deposition of chitosan in different alcohols. *J. Coat. Technol. Res.* **2014**, *11*, 739–746.

59. Jugowiec, D.; Kot, M.; Moskalewicz, T. Electrophoretic deposition and characterisation of chitosan coatings on near-β titanium alloy. *Arch. Metall. Mater.* **2016**, *61*, 657–664.

60. Rautray, T.R.; Narayanan, R.; Kim, K.H. Ion implantation of titanium based biomaterials. *Prog. Mater. Sci.* **2011**, *56*, 1137–1177.

61. Gross, K.A.; Babovic, M. Influence of abrasion on the surface characteristics of thermally sprayed hydroxyapatitae coatings. *Biomaterials* **2002**, *23*, 4731–4737.

62. Ehlert, M.; Radtke, A.; Jędrzejewski, T.; Roszek, K.; Bartmański, M.; Piszczek, P. In Vitro Studies on Nanoporous, Nanotubular and Nanosponge-Like Titania Coatings, with the Use of Adipose-Derived Stem Cells. *Materials* **2020**, *13*, 1574.

63. Alam, F.; Balani, K. Adhesion force of staphylococcus aureus on various biomaterial surfaces. *J. Mech. Behav. Biomed. Mater.* **2017**, *65*, 872–880.

64. Besra, L.; Liu, M. A review on fundamentals and applications of electrophoretic deposition (EPD). *Prog. Mater. Sci.* **2007**, *52*, 1–61.

65. Balagani, P.G.A. Formulation and evaluation of nizatidine solid dispersions. *World J. Pharm. Pharm. Sci.* **2015**, *4*, 810–817.

66. Dimzon, I.K.D.; Knepper, T.P. Degree of deacetylation of chitosan by infrared spectroscopy and partial least squares. *Int. J. Biol. Macromol.* **2015**, *72*, 939–945.

67. Menzies, K.L.; Jones, L. The impact of contact angle on the biocompatibility of biomaterials. *Optom. Vis. Sci.* **2010**, *87*, 387–399.

68. Tang, H.; Cao, T.; Liang, X.; Wang, A.; Salley, S.O.; McAllister, J.; Ng, K.Y.S. Influence of silicone surface roughness and hydrophobicity on adhesion and colonization of Staphylococcus epidermidis. *J. Biomed. Mater. Res. Part A* **2009**, *88*, 454–463.

69. Roosjen, A.; Norde, W.; Van Der Mei, H.C.; Busscher, H.J. The use of positively charged or low surface free energy coatings versus polymer brushes in controlling biofilm formation. *Prog. Colloid Polym. Sci.* **2006**, *132*, 138–144.

70. Cordero-Arias, L.; Cabanas-Polo, S.; Gao, H.; Gilabert, J.; Sanchez, E.; Roether, J.A.; Schubert, D.W.; Virtanen, S.; Boccaccini, A.R. Electrophoretic deposition of nanostructured-TiO₂/chitosan composite coatings on stainless steel. *RSC Adv.* **2013**, *3*, 11247–11254.

71. Pawłowski, Ł.; Bartmański, M.; Mielewczyk-Gryń, A.; Cieślik, B.M.; Gajowiec, G.; Zieliński, A. Electrophoretically Deposited Chitosan/Eudragit E 100/AgNPs Composite Coatings on Titanium Substrate as a Silver Release System. *Materials* **2021**, *14*, 4533.

72. Bartmanski, M.; Zielinski, A.; Jazdzewska, M.; Głodowska, J.; Kalka, P. Effects of electrophoretic deposition times and nanotubular oxide surfaces on properties of the nanohydroxyapatite/nanocopper coating on the Ti13Zr13Nb alloy. *Ceram. Int.* **2019**, *45*, 20002–20010.

73. Im, K.H.; Lee, S.B.; Kim, K.M.; Lee, Y.K. Improvement of bonding strength to titanium surface by sol-gel derived hybrid coating of hydroxyapatite and titania by sol-gel process. *Surf. Coat. Technol.* **2007**, *202*, 1135–1138.

74. Aydemir, T.; Pastore, J.I.; Jimenez-Pique, E.; Roa, J.J.; Boccaccini, A.R.; Ballarre, J. Morphological and mechanical characterization of chitosan/gelatin/silica-gentamicin/bioactive glass coatings on orthopaedic metallic implant materials. *Thin Solid Film.* **2021**, *732*, 138780.

75. Łosiewicz, B.; Maszybrocka, J.; Kubisztal, J.; Skrabalak, G.; Stwora, A. Corrosion resistance of the cpti g2 cellular lattice with tpms architecture for gas diffusion electrodes. *Materials* **2021**, *14*, 1–18.

76. Wu, S.; Wang, S.; Liu, W.; Yu, X.; Wang, G.; Chang, Z.; Wen, D. Microstructure and properties of TiO2 nanotube coatings on bone plate surface fabrication by anodic oxidation. *Surf. Coat. Technol.* **2019**, *374*, 362–373.

77. Bartmanski, M.; Zielinski, A.; Majkowska-Marzec, B.; Strugala, G. Effects of solution composition and electrophoretic deposition voltage on various properties of nanohydroxyapatite coatings on the Ti13Zr13Nb alloy. *Ceram. Int.* **2018**, *44*, 19236–19246.

78. Meng, F.; Liu, L. Electrochemical Evaluation Technologies of Organic Coatings. In *Coatings and Thin-Film Technologies*; IntechOpen: London, UK, 2019; Volume 32, pp. 137–144.

79. Tabesh, E.; Salimijazi, H.R.; Kharaziha, M.; Mahmoudi, M.; Hejazi, M. Development of an in-situ chitosan—Copper nanoparticle coating by electrophoretic deposition. *Surf. Coat. Technol.* **2019**, *364*, 239–247.

80. Karimi, A.R.; Rostaminejad, B.; Rahimi, L.; Khodadadi, A.; Khanmohammadi, H.; Shahriari, A. Chitosan hydrogels cross-linked with tris(2-(2-formylphenoxy)ethyl)amine: Swelling and drug delivery. *Int. J. Biol. Macromol.* **2018**, *118*, 1863–1870.